Supplementary Information

for

Diverse Structural Conversion and Aggregation Pathways of Alzheimer's Amyloid-β (1-40)

Yuxi Lin[1,2], Bikash R. Sahoo[3], Daisaku Ozawa[4], Misaki Kinoshita[5], Juhye Kang[6,7], Mi Hee Lim[6], Masaki Okumura[5], Yang Hoon Huh[8], Eunyoung Moon[8], Jae Hyuck Jang[8], Hyun-Ju Lee[9], Ka-Young Ryu[9], Sihyun Ham[2], Hyung-Sik Won[10], Kyoung-Seok Ryu[1], Toshihiko Sugiki[11], Jeong Kyu Bang[1], Hyang-Sook Hoe[9] Toshimichi Fujiwara[11], Ayyalusamy Ramamoorthy[3], Young-Ho Lee[1,11,12*]

[1]Protein Structure Group, Korea Basic Science Institute, Ochang, Cheongju, Chungbuk 28199, South Korea.

[2]Department of Chemistry, Sookmyung Women's University, Cheongpa-ro 47-gil 100, Yongsan-gu, Seoul 04310, South Korea.

[3]Biophysics Program and Department of Chemistry, University of Michigan, Ann Arbor, Michigan 48109-1055, United States.

[4]Department of Neurotherapeutics, Osaka University Graduate School of Medicine, 2-2 Yamadaoka, Suita, Osaka 565-0871, Japan.

[5]Frontier Research Institute for Interdisciplinary Sciences, Tohoku University, 6-3 Aramaki-Aza-Aoba, Aoba-ku, Sendai 980-8578, Japan.

[6]Department of Chemistry, Korea Advanced Institute of Science and Technology, Daejeon 34141, South Korea.

[7]Department of Chemistry, Ulsan National Institute of Science and Technology, Ulsan 44919, South Korea.

[8]Electron Microscopy Research Center, Korea Basic Science Institute, Ochang, Cheongju, Chungbuk 28199, South Korea.

[9]Department of Neural Development and Disease, Korea Brain Research Institute, 61 Cheomdan-ro, Dong-gu, Daegu, 41068, South Korea.

[10]Department of Biotechnology, Research Institute and College of Biomedical and Health Science, Konkuk University, Chungju, Chungbuk 27478, South Korea.

[11]Institute for Protein Research, Osaka University, Yamadaoka 3-2, Suita, Osaka 565-0871, Japan.
[12]Bio-Analytical Science, University of Science and Technology, Daejeon 34113, South Korea.

*To whom correspondence should be addressed: mr0505@kbsi.re.kr; mr0505@protein.osaka-u.ac.jp. (Y.-H.L.)

Table of Contents

1. Supplementary Figures

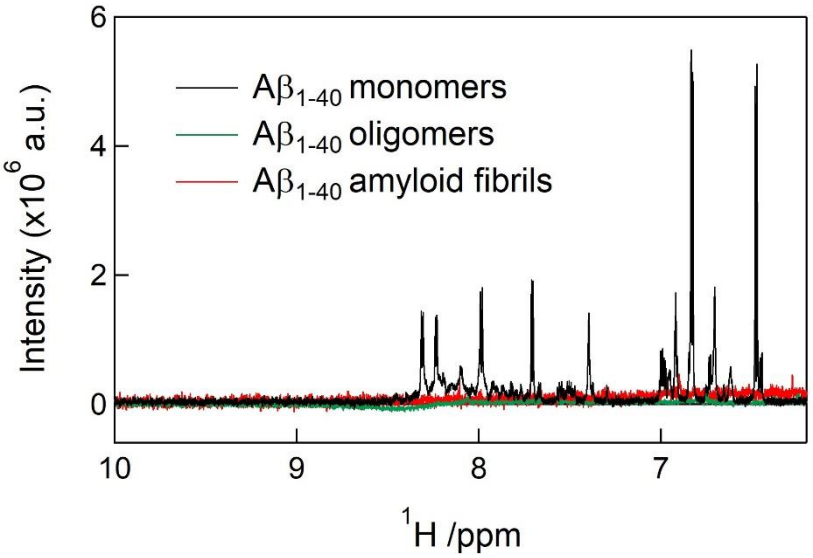

Figure S1. One dimensional proton NMR spectra of distinct molecular species of $A\beta_{1-40}$. NMR spectra of monomers (black), oligomers (green), and amyloid fibrils (red) are shown. NMR spectra were recorded on a 800 MHz NMR spectrometer equipped with a cryogenic probe (Bruker BioSpin, Germany) at 10 °C.

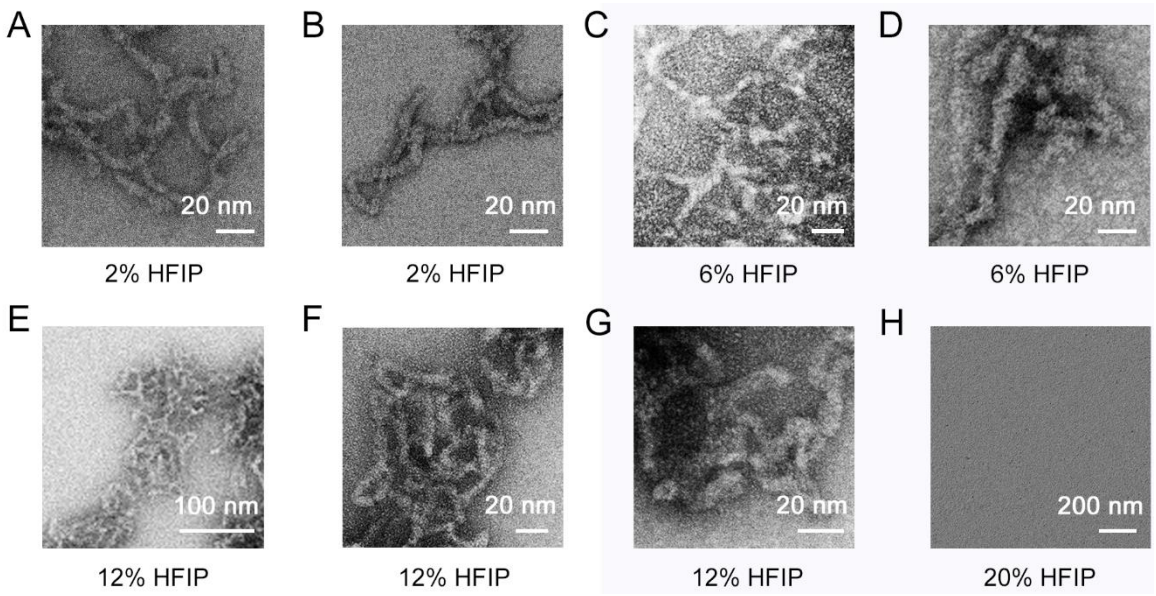

Figure S2. TEM micrographs of $A\beta_{1-40}$ at varying concentrations of HFIP. (**A**-**G**) Morphological characterization of $A\beta_{1-40}$ protofibrils formed immediately after sample preparation in (**A** and **B**) 2%, (**C** and **D**) 6%, and (**E**, **F**, and **G**) 12% HFIP. (**H**) No aggregate was detected for $A\beta_{1-40}$ in 20% HFIP. The length of each scale bar is noted.

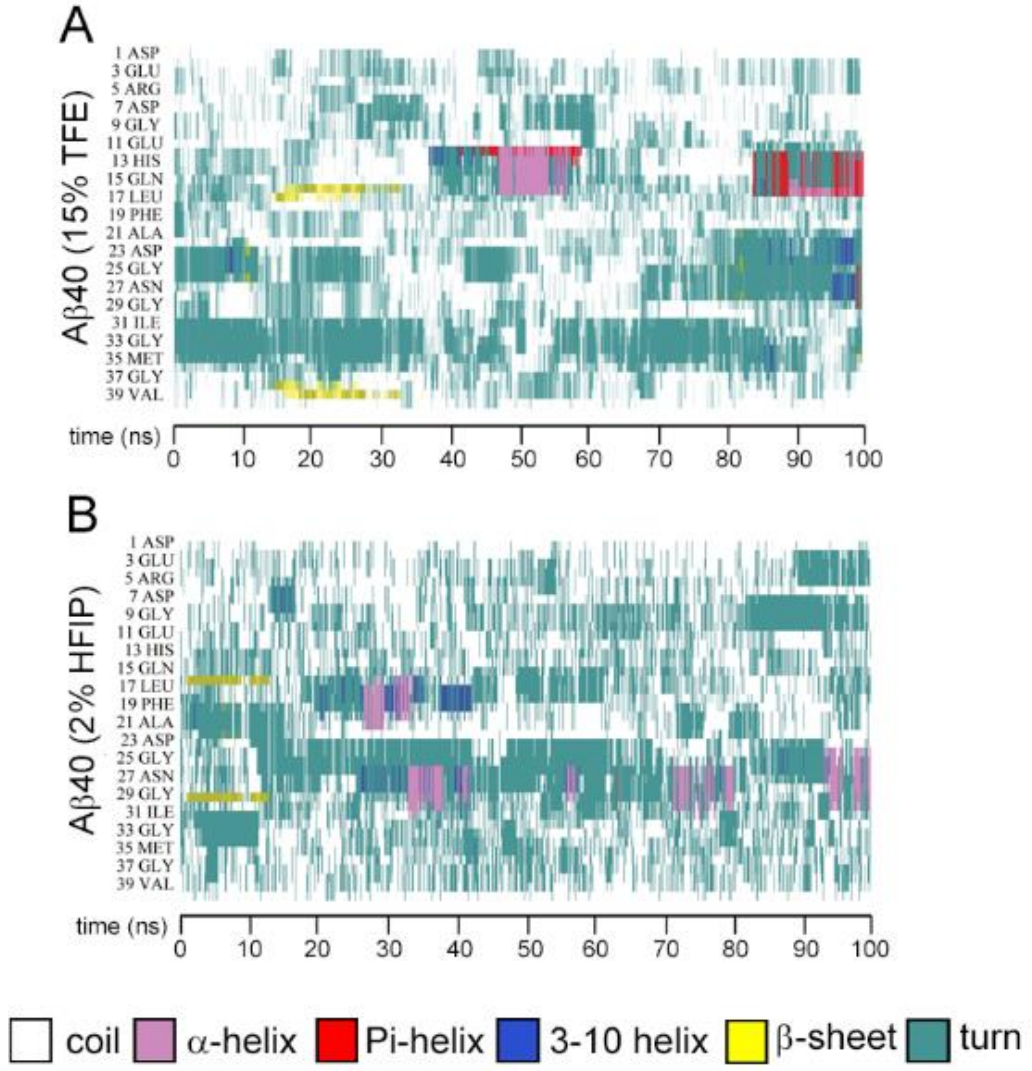

Figure S3. MD simulation of $A\beta_{1\text{-}40}$ in alcohol/water mixtures. (**A** and **B**) Secondary structure evolution maps for $A\beta_{1\text{-}40}$ in (**A**) 85% H_2O and 15% TFE as well as (**B**) 98% H_2O and 2% HFIP.

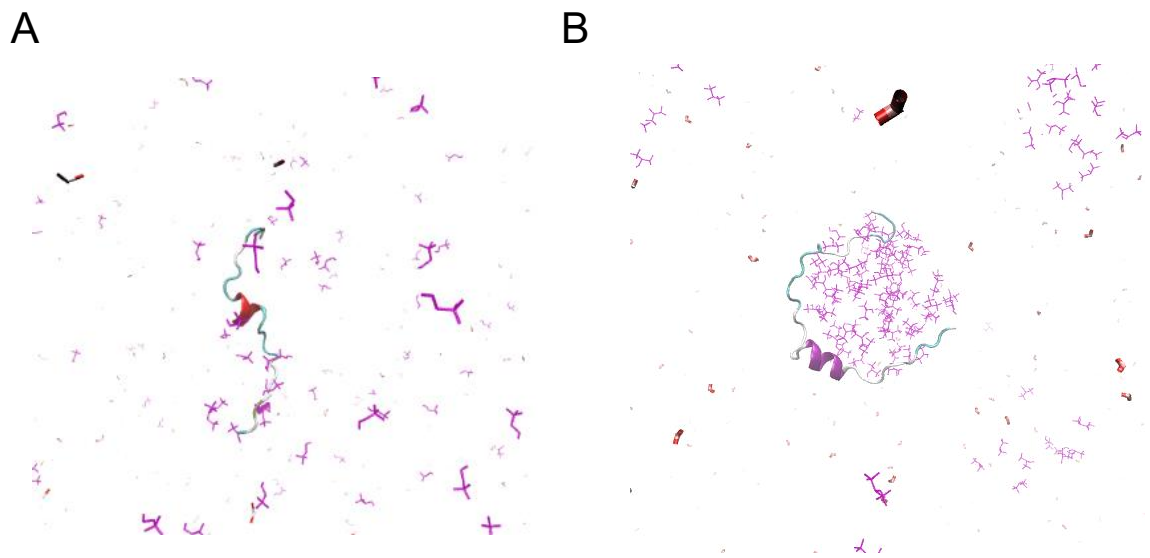

Figure S4. Characterization of interactions between $A\beta_{1-40}$ and alcohols. MD snapshots in (**A**) 85% H_2O and 15% TFE as well as (**B**) 98% H_2O and 2% HFIP are shown. $A\beta_{1-40}$, water, and alcohol molecules are represented in cartoons, bonds, and lines (purple), respectively.

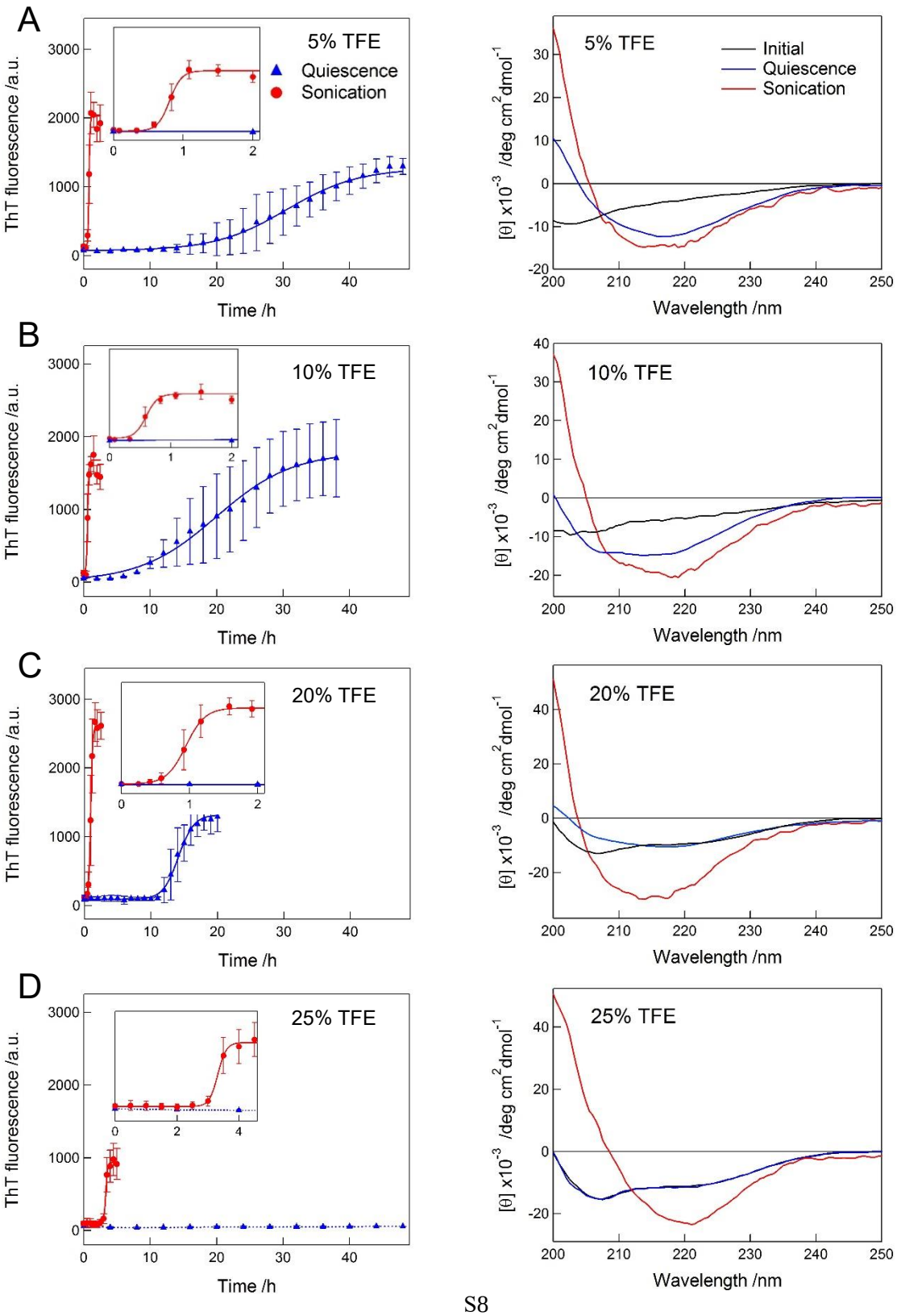
A
5% TFE
Quiescence
Sonication
ThT fluorescence /a.u.
Time /h
5% TFE
Initial
Quiescence
Sonication
[θ] x10^-3 /deg cm^2dmol^-1
Wavelength /nm
B
10% TFE
ThT fluorescence /a.u.
Time /h
10% TFE
[θ] x10^-3 /deg cm^2dmol^-1
Wavelength /nm
C
20% TFE
ThT fluorescence /a.u.
Time /h
20% TFE
[θ] x10^-3 /deg cm^2dmol^-1
Wavelength /nm
D
25% TFE
ThT fluorescence /a.u.
Time /h
25% TFE
[θ] x10^-3 /deg cm^2dmol^-1
Wavelength /nm

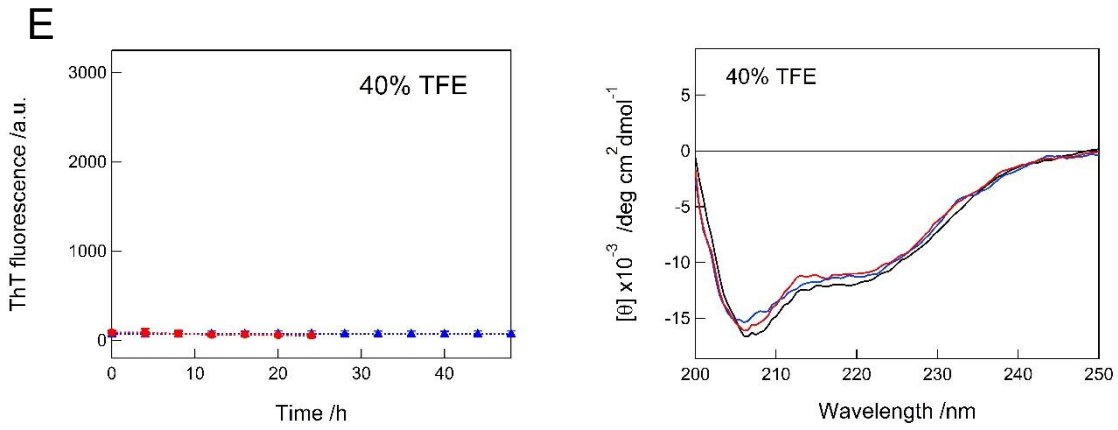

Figure S5. Monitoring of $A\beta_{1-40}$ fibrillation at various TFE concentrations with and without sonication. (**A**-**E**) The amyloid fibrillation of $A\beta_{1-40}$ was monitored by the ThT fluorescence assay (left) and far-UV CD spectroscopy (right) in (**A**) 5, (**B**) 10, (**C**) 20, (**D**) 25, and (**E**) 40% (v/v) TFE. The ThT intensity in the absence (blue triangle) and presence (red circle) of sonication was plotted as a function of incubation time. Solid lines represent the fit curves of the kinetics of $A\beta_{1-40}$ fibrillation. Dotted lines were drawn as an eye-guide only. Inserts in **A**-**D** represent the magnified profiles of rapid kinetics of $A\beta_{1-40}$ fibrillation with sonication. Error bars indicate the standard deviation from three independent measurements. The far-UV CD spectra of $A\beta_{1-40}$ after incubation with sonication (red) or without agitation (blue) were recorded. Far-UV CD spectra before incubation (black) are also shown for a comparison.

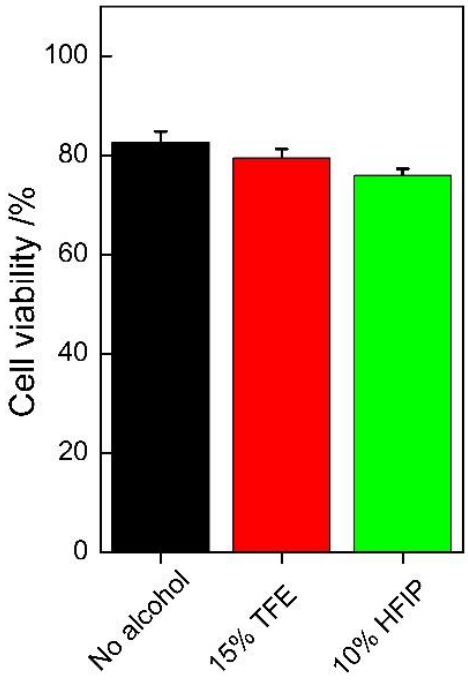

Figure S6. **Toxicity of $A\beta_{1-40}$ amyloid fibrils generated in distinct solvent conditions, monitored by the MTT assay.** SH-SY5Y cells were incubated with $A\beta_{1-40}$ amyloid fibrils formed in the absence (black) and presence of 15% TFE (red) or 10% HFIP (green) for 24 h and then cell viability was examined using UV-Vis absorbance spectroscopy. Error bars represent the standard error from three independent experiments.

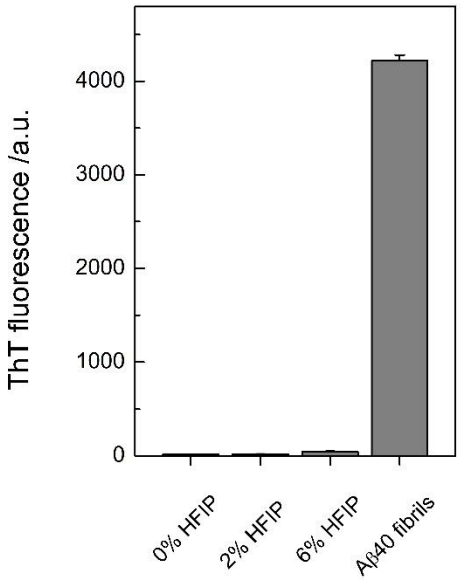

Figure S7. Examination of the effect of HFIP on the ThT fluorescence intensity. ThT fluorescence intensities of 10 mM sodium phosphate buffer (pH 7.5) containing 100 mM NaCl in 0, 2, and 6% HFIP without $A\beta_{1\text{-}40}$ peptides are shown. The ThT value of $A\beta_{1\text{-}40}$ amyloid fibrils is displayed as the control. Error bars indicate the standard deviation from three independent measurements.

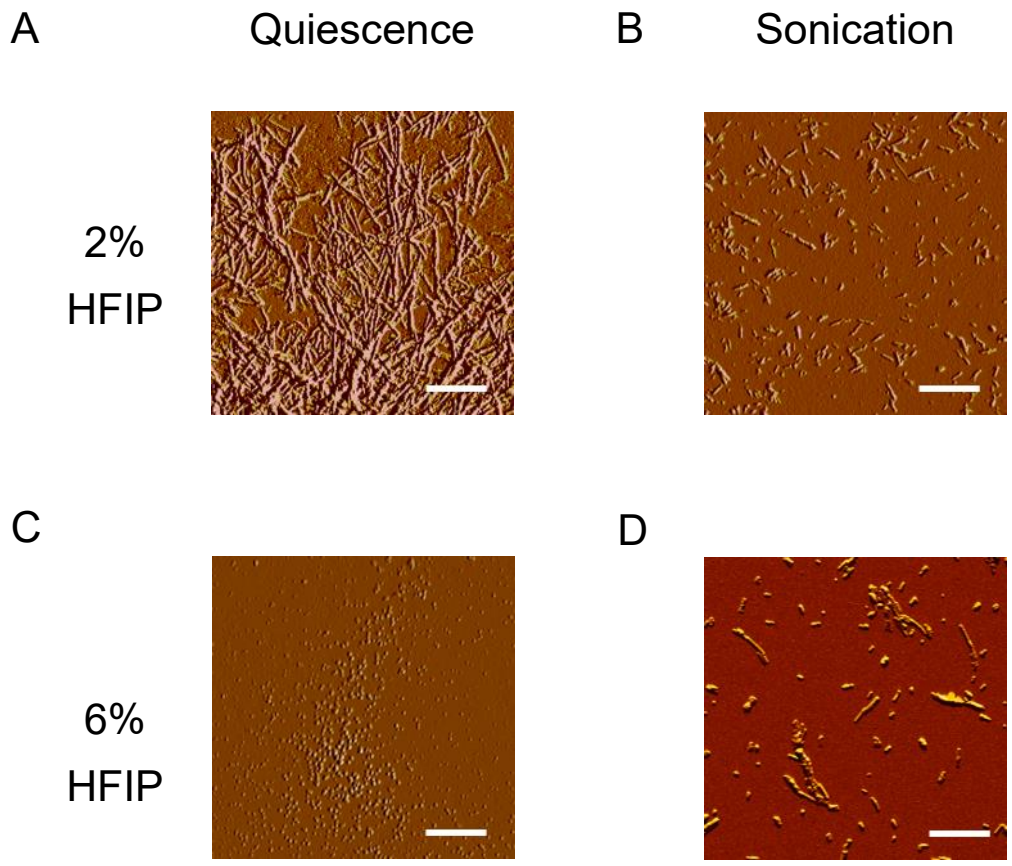

Figure S8. AFM images of HFIP-induced A$\beta_{1\text{-}40}$ aggregates. (**A**-**D**) A$\beta_{1\text{-}40}$ aggregates formed after incubation in the (**A** and **C**) absence and (**B** and **D**) presence of sonication in (**A** and **B**) 2% and (**C** and **D**) 6% HFIP. Scale bar = 500 nm.

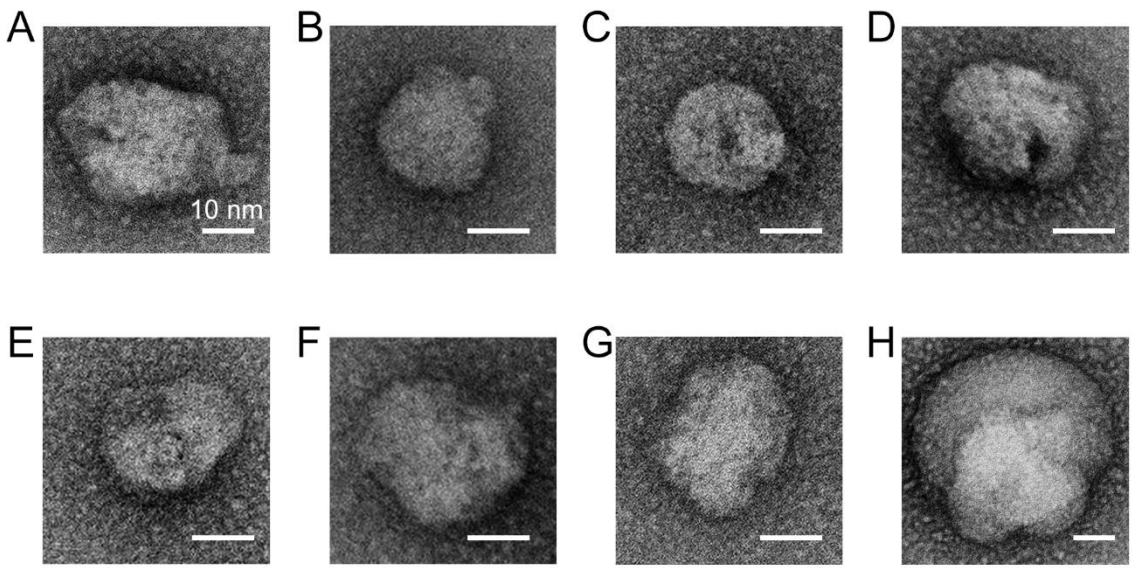

Figure S9. TEM micrographs of $A\beta_{1-40}$ oligomers. (**A**-**H**) Gallery of representative morphologies of oligomeric species of $A\beta_{1-40}$. Scale bar = 10 nm.

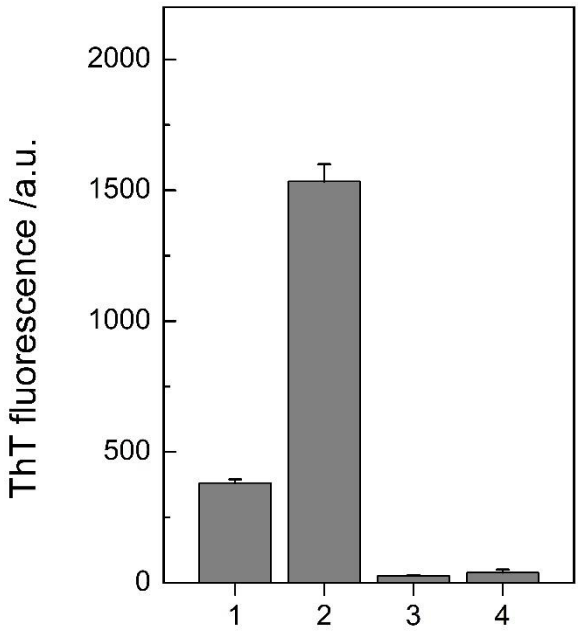

Figure S10. Examination of solvent effects on ThT fluorescence. ThT fluorescence intensities of each solution were recorded. $A\beta_{1\text{-}40}$ oligomer solution in the absence (1) and presence (2) of 10 mM sodium phosphate buffer (pH 7.5) containing 100 mM NaCl. Solution without $A\beta_{1\text{-}40}$ oligomers in the absence (3) and presence (4) of 10 mM sodium phosphate buffer (pH 7.5) containing 100 mM NaCl. The dead time for the addition of 10 mM sodium phosphate buffer (pH 7.5) containing 100 mM NaCl was ~ 20 s. Error bars indicate the standard deviation from three independent measurements.

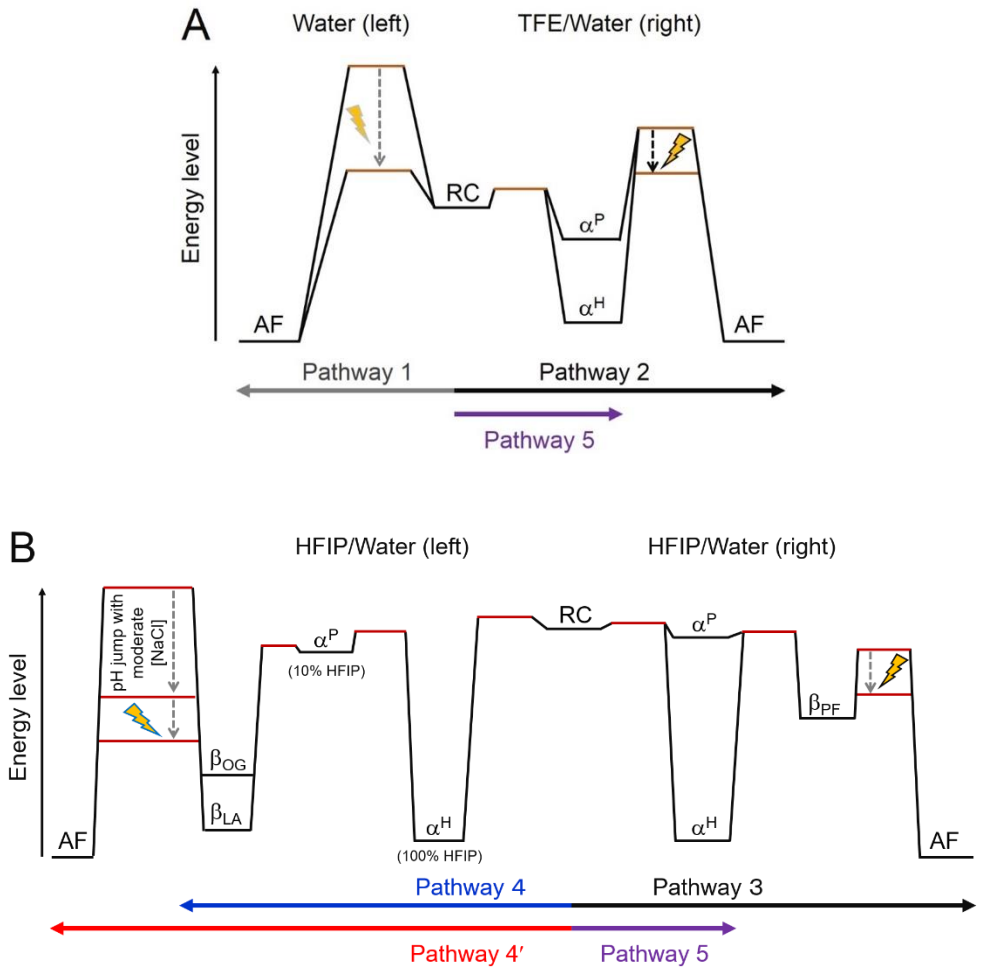

RC: Random coil structure; α^P: Partial helical structure; α^H: Highly helical structure;

β_{PF}: β-Structured protofibril; β_{OG}: β-Structured oligomer;

β_{LA}: β-Structured large aggregate; AF: Mature amyloid fibril

Figure S11. Energy landscapes of $A\beta_{1-40}$ aggregation under various conditions. (**A** and **B**) Relative energy levels and activation energy barriers are represented for buffered water without an alcohol (left), a water/TFE mixture (right) in **A**, and a water/HFIP mixture in **B**. Energy levels in

equilibria and transition states are indicated by black and brown transverse lines, respectively. The impact of sonication or a pH jump with a moderate concentration of NaCl on decreasing kinetic energy barriers is highlighted with broken and arrowed lines. Various aggregation pathways are shown below energy landscapes with distinct colors: pathway 1 (gray), pathway 2 (black), pathway 3 (green), pathway 4 (blue), pathway 4′ (red), and pathway 5 (magenta).

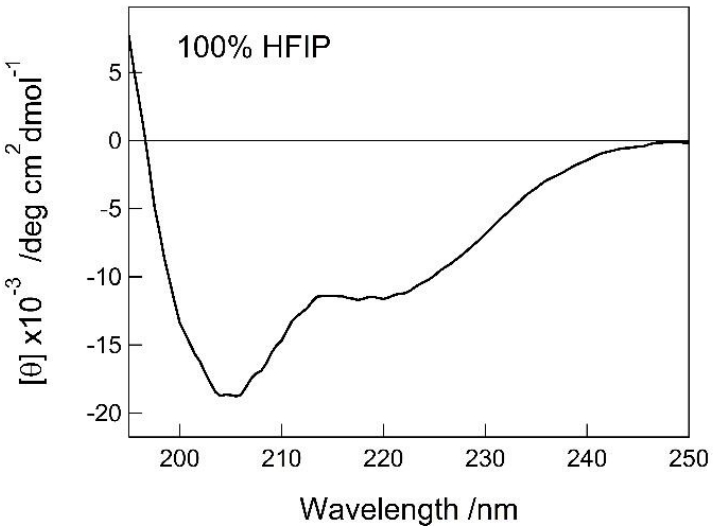

Figure S12. Secondary structure of $A\beta_{1-40}$ in 100% HFIP. The far-UV CD spectrum of $A\beta_{1-40}$ monomers dissolved in 100% HFIP is shown.

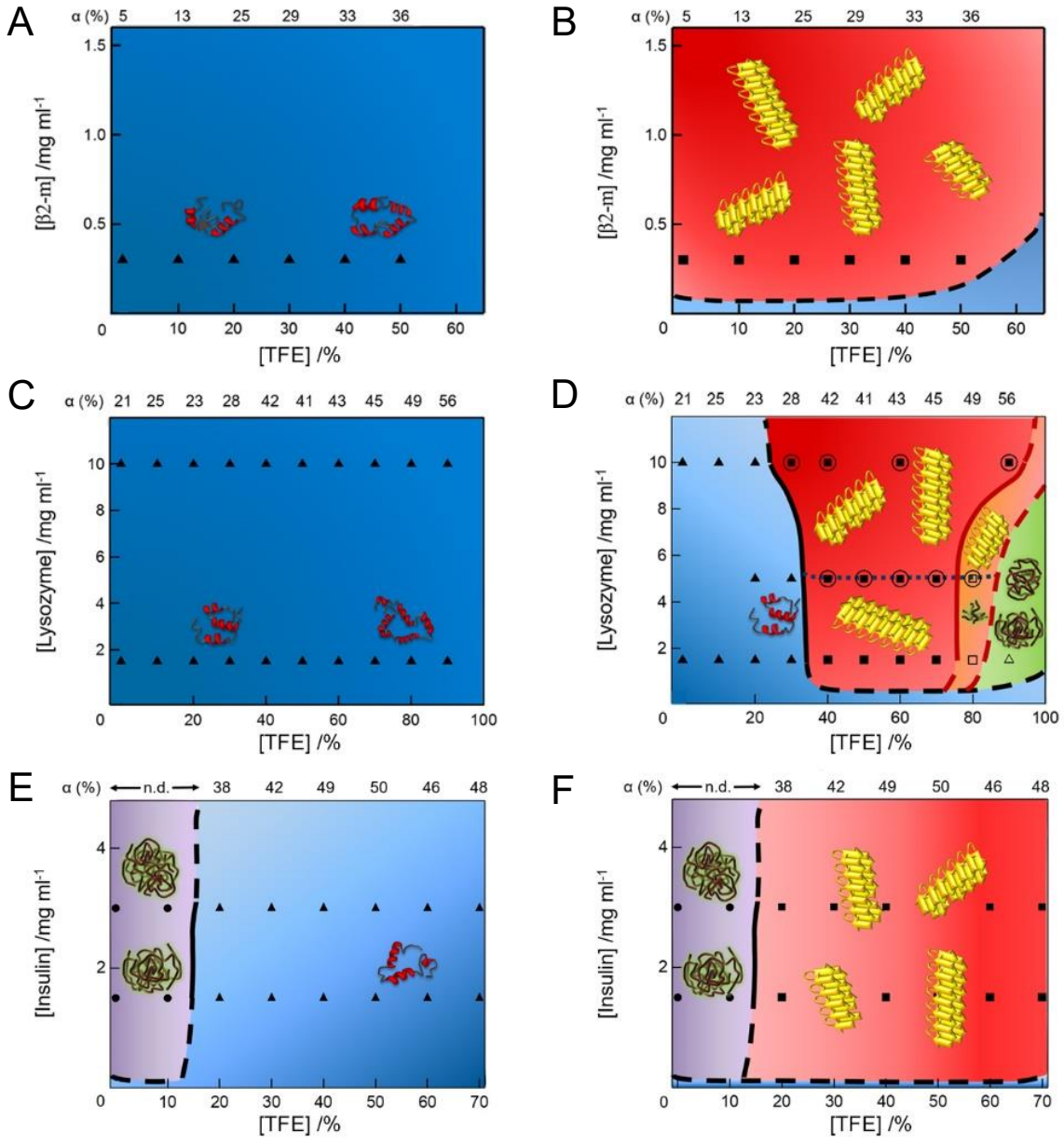

▲: Monomer ■: Mature fibril ◉: Mature fibril in a gel state

◆: Protofibrils ●: Others ◉: Others in a gel state

△: Monomer + others □: Mature fibril + others

◎: Mature fibril + other in a gel state

Others: Amorphous aggregates with small amounts of fibrils

Figure S13. Phase diagrams of the aggregation of several amyloid proteins in water/alcohol mixtures. (**A**-**F**) Phase diagrams of (**A** and **B**) β2-microglobulin, (**C** and **D**) lysozyme, and (**E** and **F**) insulin in the absence (left) and presence of sonication (right). Cartoons of helical monomers, amyloid fibrils, and amorphous aggregates are illustrated. Colors represent molecular species: (blue region) soluble monomers; (red region) mature amyloid fibrils; (magenta region in **E** and **F**) amorphous aggregates; (pink region in **D**) mainly mature amyloid fibrils with a small quantity of amorphous aggregates; (green region in **D**) monomers with a small amount of amorphous aggregates. The α-helical contents of the initial states of β2-microglobulin, lysozyme, and insulin before aggregation, analyzed by the BeStSel algorithm,[1, 2] were displayed at the top of the phase diagrams. "n.d." represents the region at which excessively fast aggregation and precipitation prevented the analysis of α-helical contents. Prior data of β2-microglobulin aggregation[3] were used for phase diagrams in **A** and **B**. Phase transitions of lysozyme[4] and insulin[5] in water/TFE mixtures were reproduced in **C**-**F** with slight modifications from our previous studies.

2. Supplementary References

1. Micsonai, A.; Wien, F.; Kernya, L.; Lee, Y. H.; Goto, Y.; Refregiers, M.; Kardos, J. Accurate Secondary Structure Prediction and Fold Recognition for Circular Dichroism Spectroscopy. *Proc. Natl. Acad. Sci. U.S.A.* **2015,** *112*, E3095-3103.
2. Micsonai, A.; Wien, F.; Bulyaki, E.; Kun, J.; Moussong, E.; Lee, Y. H.; Goto, Y.; Refregiers, M.; Kardos, J. BeStSel: A Web Server for Accurate Protein Secondary Structure Prediction and Fold Recognition from the Circular Dichroism Spectra. *Nucleic Acids Res.* **2018,** *46*, W315-W322.
3. Chatani, E.; Yagi, H.; Naiki, H.; Goto, Y. Polymorphism of β_2-Microglobulin Amyloid Fibrils Manifested by Ultrasonication-Enhanced Fibril Formation in Trifluoroethanol. *J. Biol. Chem.* **2012,** *287*, 22827-22837.
4. Lin, Y.; Lee, Y. H.; Yoshimura, Y.; Yagi, H.; Goto, Y. Solubility and Supersaturation-Dependent Protein Misfolding Revealed by Ultrasonication. *Langmuir* **2014,** *30*, 1845-1854.
5. Muta, H.; Lee, Y. H.; Kardos, J.; Lin, Y.; Yagi, H.; Goto, Y. Supersaturation-Limited Amyloid Fibrillation of Insulin Revealed by Ultrasonication. *J. Biol. Chem.* **2014,** *289*, 18228-18238.